

Time-Varying Hazard Patterns and Co-Mutation Profiles of KRAS G12C and G12D in Real-World NSCLC

Robert Amevor^{*1}, Emmanuel Kubuafor², and Dennis Baidoo²

¹Arnold School of Public Health, University of South Carolina, Columbia, SC, USA

²Department of Mathematics and Statistics, University of New Mexico, Albuquerque, NM, USA

Abstract

Background: KRAS mutations represent the largest oncogenic subset in non-small cell lung cancer (NSCLC), yet allele-specific clinical behavior in real-world settings remains incompletely characterized. While KRAS G12C is now targetable with approved inhibitors, no equivalent agents exist for G12D. We examined time-to-next-treatment (TTNT) and overall survival (OS) differences between KRAS G12C and G12D using harmonized clinical-genomic data, allowing for time-varying hazard effects.

Methods: De-identified data from the AACR Project GENIE BioPharma Collaborative (BPC) NSCLC v2.0-public release were analyzed. TTNT served as a pragmatic real-world surrogate for progression-free survival, derived from curated systemic therapy timelines. Co-alterations in *TP53*, *STK11*, *KEAP1*, *SMARCA4*, and *MET* were harmonized across mutation, copy-number, and structural variant data. Kaplan–Meier, multivariable Cox, time-dependent Cox, and a pre-specified piecewise Cox model (split at median TTNT = 23.0 months) were applied. Proportional hazards were assessed via Schoenfeld residuals; nonparametric bootstrap resampling ($B = 1000$) evaluated stability of time-varying estimates.

Results: The TTNT cohort comprised 162 patients (G12C $n = 130$; G12D $n = 32$). Median TTNT was 28.6 months for G12C versus 32.0 months for G12D (log-rank $p = 0.79$). Adjusted Cox regression showed no overall TTNT hazard difference ($HR_{G12D \text{ vs } G12C} = 0.85$; 95% CI 0.53–1.37; $p = 0.50$). Schoenfeld testing indicated borderline non-proportionality for KRAS ($p = 0.053$). Piecewise Cox modeling revealed a time-varying pattern: an early

*Corresponding author: ramevor@email.sc.edu

TTNT hazard favoring G12D ($HR_{\text{early}} = 0.41$; 95% CI 0.17–0.97; $p = 0.043$) with a statistically significant $KRAS \times \text{period}$ interaction ($HR = 3.33$; 95% CI 1.19–9.31; $p = 0.021$) and attenuation in the late period ($HR_{\text{late}} = 1.38$; 95% CI 0.77–2.47; $p = 0.285$). Bootstrap resampling confirmed these patterns (median $HR_{\text{early}} = 0.39$; median $HR_{\text{late}} = 1.41$). Among 278 OS-evaluable patients (133 deaths), multivariable Cox regression indicated improved OS for G12D (adjusted $HR = 0.63$; 95% CI 0.39–0.99; $p = 0.048$). $KRAS$ G12C tumors exhibited higher median TMB (9.79 vs. 7.83 mut/Mb; $p = 0.002$) and greater enrichment of *STK11* and *KEAP1* co-mutations.

Conclusions: $KRAS$ G12D and G12C demonstrate distinct temporal treatment trajectories in this multi-institutional real-world cohort. G12D was associated with an early TTNT advantage and improved overall survival; these patterns were directionally consistent across bootstrap and sensitivity analyses. The late-period TTNT difference did not reach statistical significance, likely reflecting limited power (post-hoc power: 12.3%) given the small G12D cohort. These findings are exploratory and hypothesis-generating, requiring prospective validation in larger, allele-resolved cohorts. They nonetheless support continued investigation of allele-specific biology and dedicated therapeutic development for $KRAS$ G12D.

Keywords: $KRAS$ G12C; $KRAS$ G12D; non-small cell lung cancer; time-to-next-treatment; overall survival; time-varying hazards; piecewise Cox regression; tumor mutational burden; AACR Project GENIE.

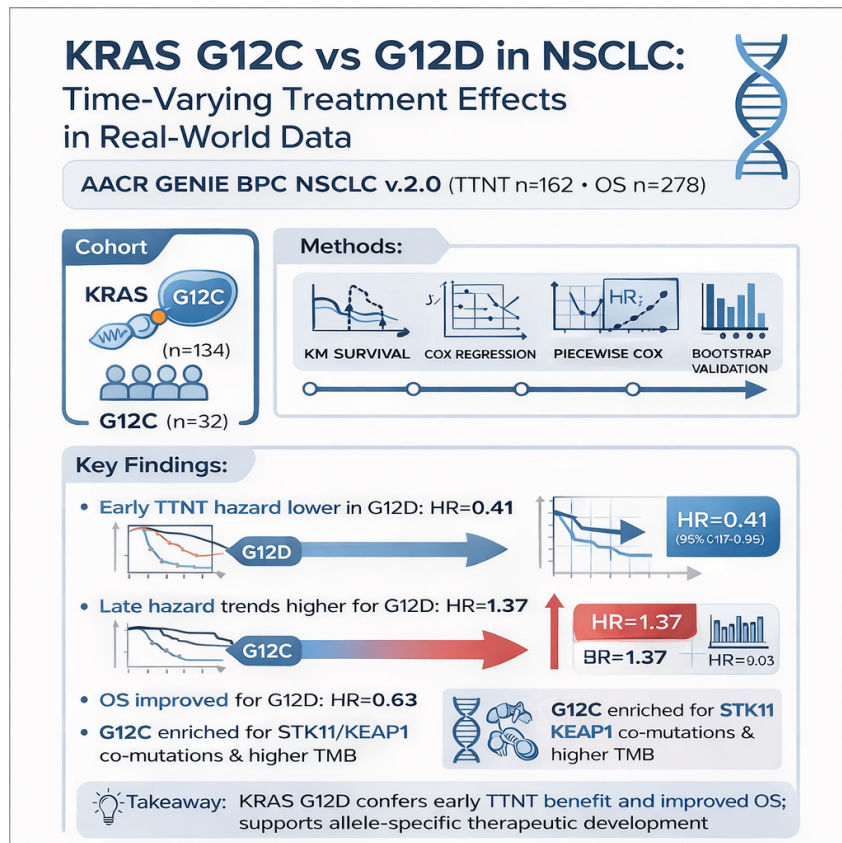


Figure 1: Graphical result

1 Introduction

KRAS mutations are the most prevalent oncogenic drivers in non-small cell lung cancer (NSCLC), occurring in approximately 25–30% of lung adenocarcinomas worldwide [Frisch et al., 2025, Lim et al., 2023]. Among these, the glycine-to-cysteine substitution (G12C) accounts for approximately 13% of all NSCLC cases, while codon-12 variants including G12D, G12V, and G12S contribute to the remaining molecular heterogeneity [Shahnam et al., 2025]. This allele-level heterogeneity is clinically meaningful: KRAS substitutions differ in downstream biochemical signaling, co-mutation profiles, tumor immune microenvironment (TIME) characteristics, and sensitivity to therapeutic agents [Zhang et al., 2022, Bazhenova, 2023].

The development of allele-specific KRAS G12C inhibitors has transformed treatment options for this molecular subgroup. Sotorasib and adagrasib have produced clinically meaningful response rates and progression-free survival benefits in previously treated KRAS G12C NSCLC [Skoulidis et al., 2021, Jänne et al., 2022], and next-generation agents such as divarasib continue to expand the landscape [Brazel and Nagasaka, 2024]. By contrast, no approved targeted therapies exist for KRAS G12D, although early-phase G12D-directed agents including zoldonrasib have shown preliminary activity [Hippensteele]. These divergent therapeutic trajectories underscore the importance of characterizing allele-specific clinical behavior in real-world populations.

Real-world evidence suggests that allele-specific outcomes may be substantially modified by co-occurring genomic alterations. KRAS G12C tumors frequently exhibit higher tumor mutational burden (TMB), tobacco-related mutational signatures, and enriched baseline immunogenicity relative to non-G12C alleles [Zhao et al., 2024, Geçgel et al., 2025]. Concurrently, alterations in *STK11*, *KEAP1*, and *SMARCA4* define immunologically cold phenotypes with attenuated benefit from immune checkpoint blockade (ICB) [Bazhenova, 2023], and these co-mutations occur at differing frequencies across KRAS alleles [Galan-Cobo et al., 2025, Zhang et al., 2022].

Most existing retrospective studies of KRAS allele outcomes rely on static survival comparisons or trial-enriched cohorts, limiting real-world generalizability [Shahnam et al., 2025]. Importantly, conventional Cox proportional-hazards models assume a constant hazard ratio over the entire follow-up period; if allele-specific effects are time-varying, such analyses may obscure clinically meaningful dynamics. Time-to-next-treatment (TTNT) has emerged as a pragmatic and validated real-world surrogate for progression-free survival in observational oncology datasets, permitting longitudinal assessment of treatment durability [de Bruijn et al., 2023, Khozin et al., 2019, Campbell et al., 2020].

The AACR Project GENIE BioPharma Collaborative (BPC) NSCLC dataset provides a uniquely comprehensive platform for allele-resolved, time-adaptive outcome analyses, integrating harmonized multi-institutional clinical timelines with matched genomic profiles [GEN, 2023, de Bruijn et al., 2023]. Using this resource, we sought to: (1) compare TTNT and OS between KRAS G12C and G12D in a real-world multi-institutional cohort; (2) evaluate whether allele-specific hazards are time-varying using piecewise and time-dependent Cox models; and (3) characterize allele-specific co-mutation profiles and assess their relationship to outcomes.

2 Methods

2.1 Data Source

De-identified clinical and genomic data were obtained from the AACR Project GENIE BioPharma Collaborative (BPC) NSCLC v2.0-public release, accessed through cBioPortal [de Bruijn et al., 2023, AACR Project GENIE Consortium, 2017]. This dataset includes harmonized clinical annotations, curated systemic treatment timelines, and linked somatic mutation, copy-number alteration, and structural variant files for patients treated at multiple U.S. academic cancer centers. Because all data are fully de-identified, this analysis was exempt from institutional review board oversight.

2.2 Cohort Construction

Patients were included if they had: (1) a diagnosis of lung adenocarcinoma; (2) a confirmed somatic KRAS p.G12C or p.G12D mutation on next-generation sequencing; and (3) evaluable systemic therapy timelines enabling derivation of TTNT. Patients lacking therapy start dates, missing TTNT event indicators, or without linked genomic data were excluded. OS analyses used available diagnosis-to-death timelines and harmonized vital status fields. Cohort construction is summarized in Figure 2.

2.3 Endpoint Definitions

Time-to-Next-Treatment (TTNT). TTNT served as the primary real-world endpoint and pragmatic surrogate for progression-free survival [Khozin et al., 2019, Campbell et al., 2020]. TTNT was defined as the maximum recorded duration across all systemic therapy episodes in GENIE BPC. The event indicator was the initiation of a subsequent regimen (number of cancer-directed regimens > 1); patients on a single regimen were censored at last follow-up. This definition reflects clinician-assessed treatment failure or progression necessitating a regimen

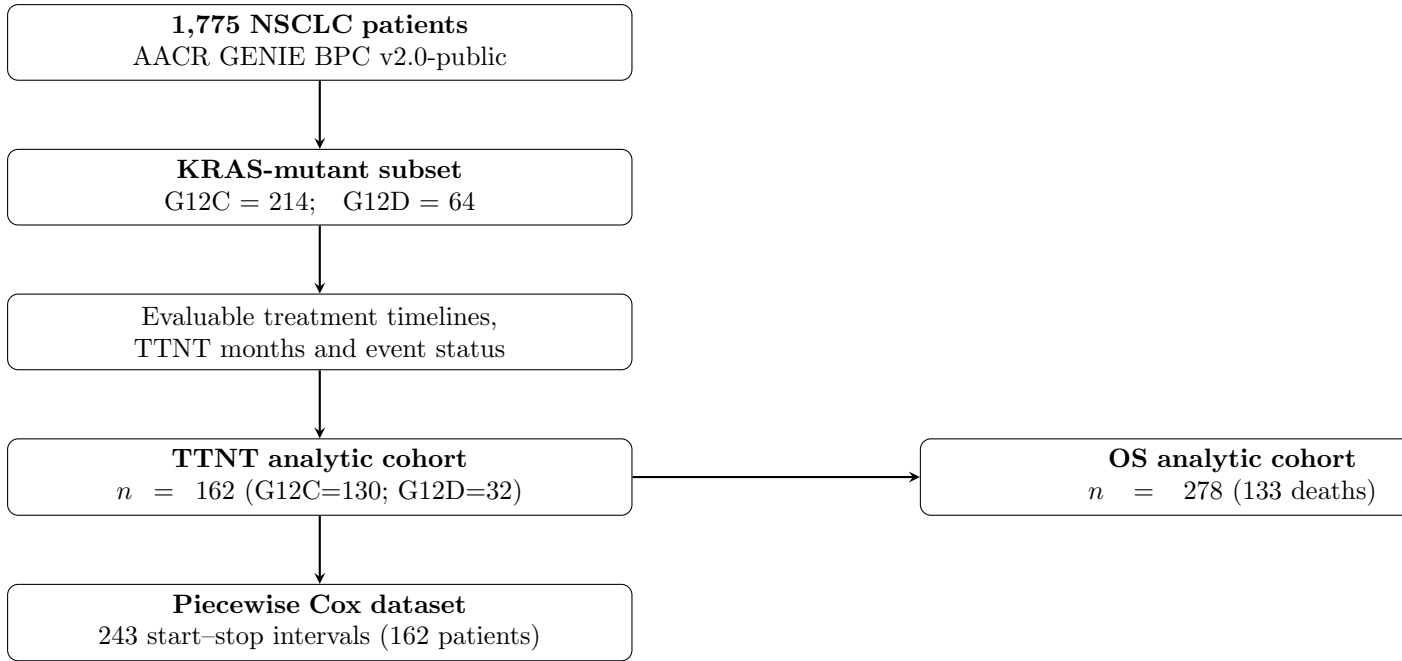


Figure 2: CONSORT-style flow diagram of patient selection for TTNT and OS analyses.

change.

Overall Survival (OS). OS was measured from the date of pathological diagnosis to death or last known contact. Vital status was derived from harmonized “OS Status from start of [therapy]” fields across all curated treatment lines; a patient was classified as deceased if any field indicated “1:DECEASED o.”

2.4 Genomic Variable Harmonization

Binary alteration indicators for five co-mutation genes of clinical interest (*TP53*, *STK11*, *KEAP1*, *SMARCA4*, *MET*) were derived by merging mutation, copy-number alteration, and structural variant tables. A gene was considered altered if any data source indicated a non-wild-type call; samples with missing data were conservatively assigned wild-type status. TMB was extracted from the curated nonsynonymous mutation count field and analyzed as a continuous variable. PD-L1 positivity was binarized (positive vs. negative/unknown) using harmonized institutional report values.

2.5 Statistical Analysis

2.5.1 Descriptive and Comparative Analyses

Baseline characteristics were summarized by allele group using medians for continuous variables and proportions for categorical variables. Between-group differences were assessed with

Wilcoxon rank-sum tests (continuous) and Fisher’s exact tests (categorical).

2.5.2 Kaplan–Meier and Standard Cox Models

Unadjusted TTNT and OS were compared using Kaplan–Meier curves and log-rank tests. Multivariable Cox proportional-hazards models were adjusted for age at sequencing, sex, and *STK11* and *TP53* co-mutation status. Proportional hazards assumptions were assessed using Schoenfeld residuals for each covariate and globally.

2.5.3 Time-Varying Hazard Models

Because KRAS exhibited borderline non-proportionality (Schoenfeld $p = 0.053$), two complementary time-adaptive approaches were applied:

Time-dependent Cox model. A $\text{KRAS} \times \log(t)$ interaction term was fitted to quantify continuous temporal change in the allele-specific hazard, without imposing a fixed cut-point.

Pre-specified piecewise Cox model. Follow-up time was partitioned at the median TTNT (23.0 months), a cut-point selected *a priori* based on the distribution of follow-up times rather than outcome-dependent optimization, thereby avoiding data-driven selection bias. Using the counting-process data structure, each patient contributed one or two start–stop intervals ($[0, c]$ and $(c, T_i]$). The $\text{KRAS} \times \text{Period}$ interaction term quantified the change in allele-specific hazard between early and late intervals. Period-specific HRs and 95% confidence intervals were derived using the delta method.

2.5.4 Bootstrap Internal Validation

To assess the robustness of early and late HR estimates, nonparametric bootstrap resampling was performed ($B = 1000$ iterations). In each iteration, patients were resampled with replacement at the patient level, the piecewise Cox model was refit, and period-specific HRs were extracted. Results were summarized as medians and 95% percentile confidence intervals across bootstrap replicates.

2.5.5 Sensitivity Analyses

Pre-specified sensitivity analyses included: (1) adjustment for TMB (per 5 mut/Mb) to evaluate potential confounding by mutational burden; (2) alternative piecewise cut-points at the 25th, 75th, and 95th TTNT percentiles to assess cut-point dependence; and (3) exclusion of treatment changes within 2 months to reduce administrative censoring bias.

All analyses were performed in R (version 4.3.1) using the `survival`, `survminer`, `flexsurv`, `dplyr`, and `ggplot2` packages [Therneau, 2023, Kassambara et al., 2019, Wickham et al., 2023].

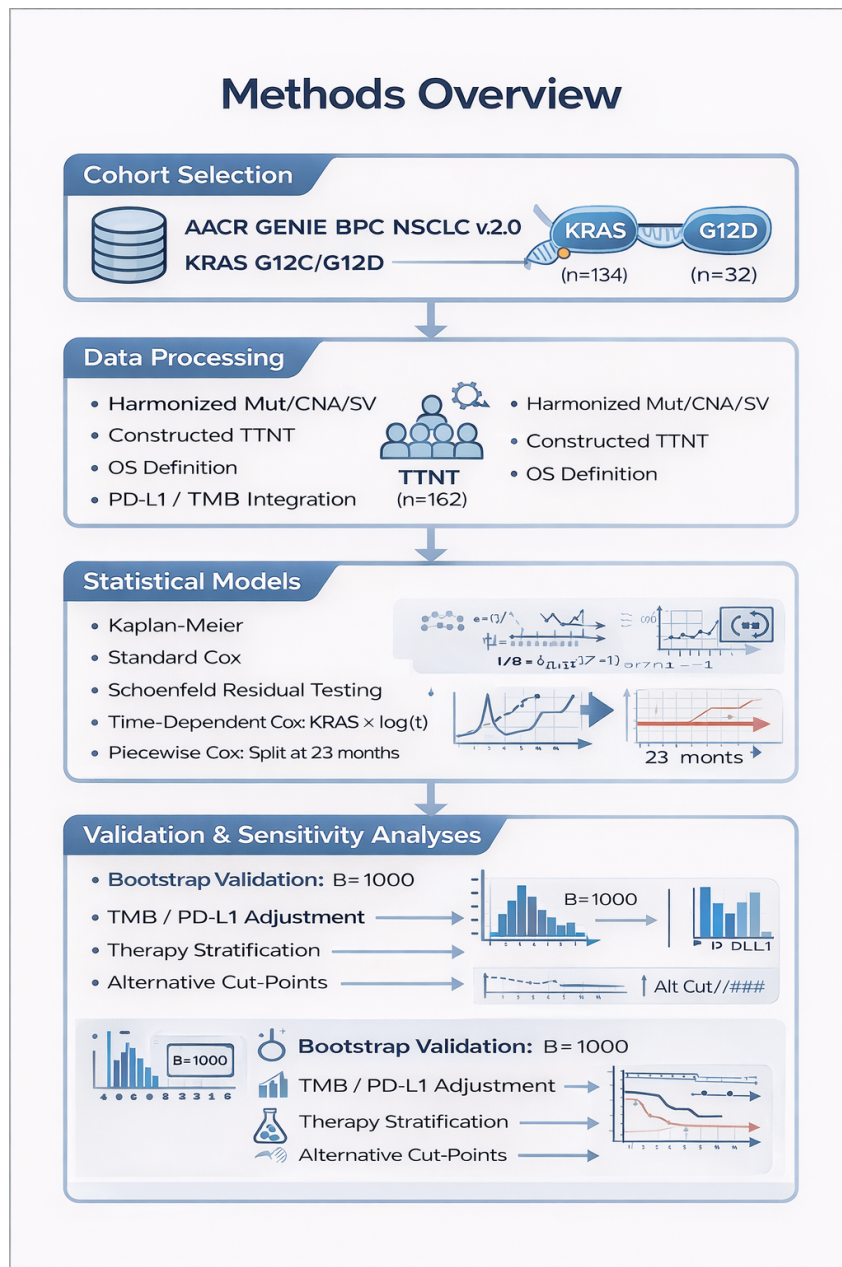


Figure 3

3 Results

3.1 Cohort Characteristics and Molecular Features

Of 1,775 NSCLC patients in the AACR GENIE BPC v2.0-public dataset, 278 patients with KRAS G12C ($n = 214$) or KRAS G12D ($n = 64$) mutations had evaluable OS data and formed the molecular characterization cohort. A subset of 162 patients met all criteria for TTNT analysis (G12C $n = 130$; G12D $n = 32$; Table 1).

KRAS G12C tumors showed significantly higher median TMB (9.79 vs. 7.83 mut/Mb; Wilcoxon $p = 0.002$) and greater co-mutation enrichment in *STK11* (31.8% vs. 17.2%; Fisher’s $p = 0.027$). *KEAP1* alteration showed a similar directional trend (18.7% vs. 9.4%; $p = 0.087$). *TP53*, *SMARCA4*, and *MET* frequencies did not differ significantly between alleles. PD-L1 positivity rates were comparable (57% G12C vs. 50% G12D; $p = 0.623$).

Table 1: Baseline clinical and genomic characteristics by KRAS allele (OS cohort, $n = 278$). The TTNT cohort ($n = 162$) is a subset with complete treatment timeline data. TMB = tumor mutational burden; PD-L1 = programmed death-ligand 1. Continuous variables compared by Wilcoxon rank-sum test; categorical variables by Fisher’s exact test.

Characteristic	G12C ($n = 214$)	G12D ($n = 64$)	Total ($N = 278$)	p -value
Sex: male, n (%)	82 (38.3%)	19 (29.7%)	101 (36.3%)	0.238
TMB, median (mut/Mb)	9.79	7.83	9.40	0.002
PD-L1 positive (%)	49 (57.0%)	10 (50.0%)	59 (55.1%)	0.623
any- <i>STK11</i> (%)	68 (31.8%)	11 (17.2%)	79 (28.4%)	0.027
any- <i>TP53</i> (%)	92 (43.0%)	27 (42.2%)	119 (42.8%)	1.000
any- <i>KEAP1</i> (%)	40 (18.7%)	6 (9.4%)	46 (16.5%)	0.087
any- <i>SMARCA4</i> (%)	27 (12.6%)	5 (7.8%)	32 (11.5%)	0.375
any- <i>MET</i> (%)	21 (9.8%)	3 (4.7%)	24 (8.6%)	0.309

3.2 TTNT: Kaplan–Meier and Multivariable Cox Analyses

Kaplan–Meier analysis demonstrated no significant overall TTNT difference between alleles (Figure 4). Median TTNT was 28.6 months (95% CI: 24.9–34.7) for G12C versus 32.0 months (95% CI: 23.9–45.4) for G12D (log-rank $p = 0.787$).

In multivariable Cox regression adjusting for age, sex, *STK11*, and *TP53*, KRAS allele subtype was not significantly associated with overall TTNT hazard ($HR_{G12D \text{ vs } G12C} = 0.85$; 95% CI 0.53–1.37; $p = 0.50$; Table 2). *STK11* alteration showed a directional trend toward shorter TTNT ($HR = 1.30$; 95% CI 0.85–1.99; $p = 0.23$) consistent with published literature, though it did not reach statistical significance in this sample.

Schoenfeld residual testing indicated borderline non-proportionality for the KRAS term ($p_{KRAS} = 0.053$; global $p = 0.334$), motivating additional time-adaptive modeling.

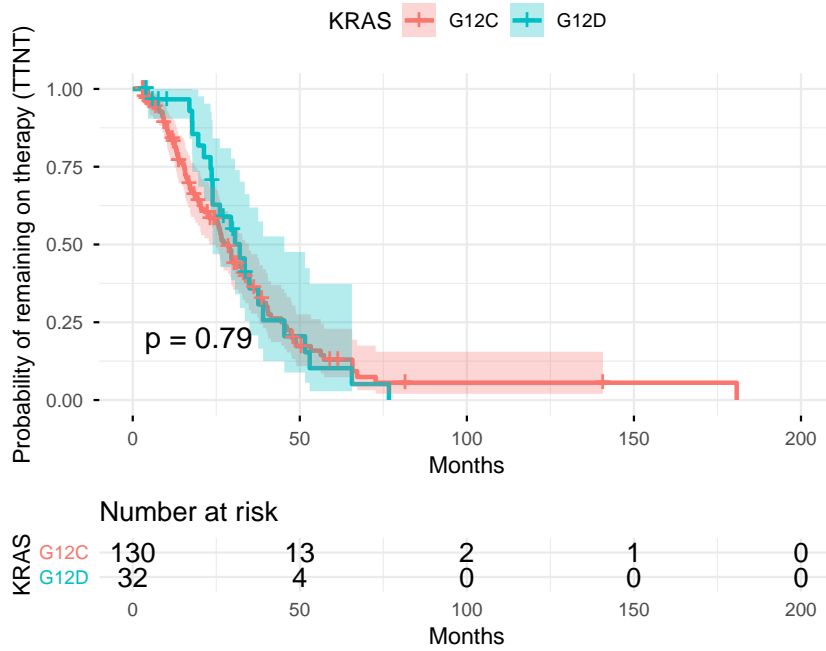


Figure 4: Kaplan–Meier curves for time-to-next-treatment (TTNT) by KRAS allele (G12C $n = 130$; G12D $n = 32$). Median TTNT: 28.6 vs. 32.0 months; log-rank $p = 0.787$.

Table 2: Multivariable Cox proportional-hazards model for TTNT.

Variable	HR	95% CI	p -value
KRAS G12D vs G12C	0.85	0.53–1.37	0.50
Age (per year)	1.01	0.99–1.03	0.55
Sex: Female (ref: Male)	1.35	0.87–2.10	0.18
<i>STK11</i> altered	1.30	0.85–1.99	0.23
<i>TP53</i> altered	0.77	0.52–1.15	0.20

3.3 Time-Varying Hazard Analysis

3.3.1 Piecewise Cox Model

The pre-specified piecewise Cox model (cut at median TTNT = 23.0 months) generated 243 start–stop intervals from 162 patients contributing 114 events. The model revealed a time-varying hazard pattern (Table 3; Figure 5).

During the early interval (0–23 months), G12D was associated with a lower TTNT hazard compared with G12C ($HR_{\text{early}} = 0.41$; 95% CI 0.17–0.97; $p = 0.043$). A statistically significant KRAS \times Period interaction ($HR = 3.33$; 95% CI 1.19–9.31; $p = 0.021$) indicated that this early difference did not persist: the late-period HR was 1.38 (95% CI 0.77–2.47; $p = 0.285$), with the confidence interval crossing unity and not reaching statistical significance. The interaction indicates a directional shift in the relative hazard between periods, though late-period estimates should be interpreted with caution given their imprecision (see Limitations). Overall model fit

was supported by concordance = 0.614 (SE = 0.029) and a significant likelihood ratio test ($p = 0.04$).

Complementary time-dependent Cox modeling using a $\text{KRAS} \times \log(t)$ interaction produced directionally consistent findings, confirming that the temporal pattern is not an artifact of the specific 23-month cut-point choice.

Table 3: Piecewise Cox model for TTNT. The KRAS coefficient represents the early-period HR; the late-period HR (1.38; 95% CI 0.77–2.47) is derived from the sum of the KRAS and interaction coefficients using the delta method.

Variable	HR	95% CI	p -value
KRAS G12D (early period)	0.41	0.17–0.97	0.043
Age (per year)	1.01	0.99–1.03	0.532
Sex (Male vs Female)	0.73	0.47–1.12	0.149
<i>STK11</i> altered	1.22	0.79–1.89	0.359
<i>TP53</i> altered	0.78	0.52–1.17	0.225
KRAS \times late period	3.33	1.19–9.31	0.021

$n = 162$ patients; events = 114; concordance = 0.614 (SE = 0.029)
Likelihood ratio $p = 0.04$; Wald $p = 0.05$; Score $p = 0.05$
Late-period KRAS HR (delta method): 1.38 (95% CI 0.77–2.47; $p = 0.285$)

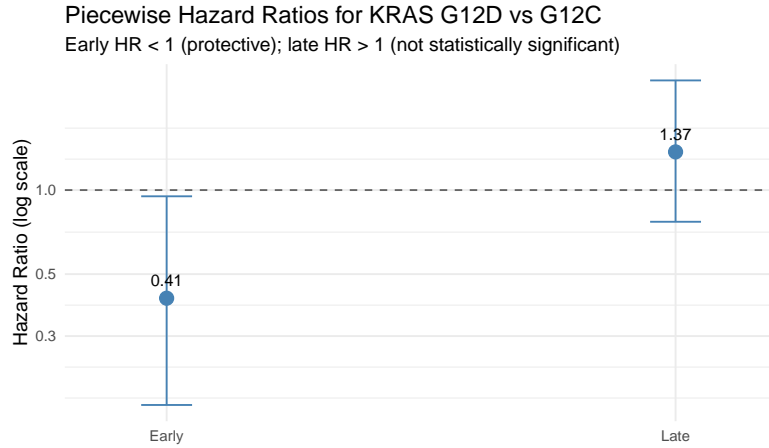


Figure 5: Period-specific hazard ratios for KRAS G12D vs G12C from the piecewise Cox model (cut-point: 23 months). $\text{HR}_{\text{early}} = 0.41$ (95% CI 0.17–0.97); $\text{HR}_{\text{late}} = 1.38$ (95% CI 0.77–2.47). Dashed line at HR = 1.0. Late-period HR did not reach statistical significance ($p = 0.285$).

3.3.2 Bootstrap Validation

Nonparametric bootstrap resampling ($B = 1000$) at the patient level confirmed the directional stability of the time-varying pattern (Figure 6). Bootstrap-derived HR distributions yielded median $\text{HR}_{\text{early}} = 0.39$ (95% percentile interval: 0.11–0.87) and median $\text{HR}_{\text{late}} = 1.41$ (95% percentile interval: 0.75–3.24). The close agreement between point estimates and bootstrap

medians supports the internal robustness of the observed pattern. The wider percentile interval for the late HR reflects genuine uncertainty arising from the limited G12D sample size (see Limitations).

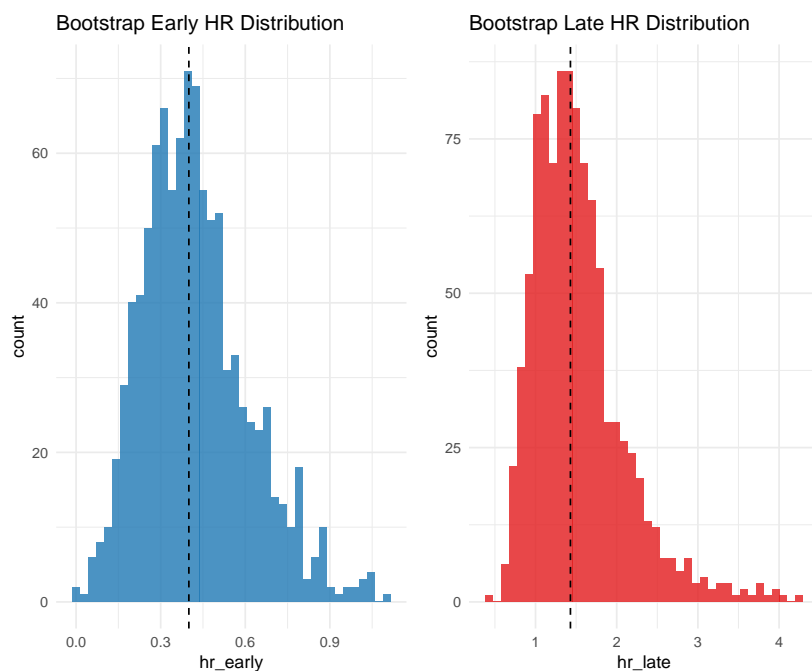


Figure 6: Bootstrap distributions ($B = 1000$ resamples) for early and late period-specific hazard ratios. Median $HR_{\text{early}} = 0.39$ (95% PI: 0.11–0.87); median $HR_{\text{late}} = 1.41$ (95% PI: 0.75–3.24). Dashed vertical lines indicate medians; solid red lines indicate $HR = 1$.

3.4 Overall Survival

Among 278 OS-evaluable patients (G12C $n = 214$; G12D $n = 64$; 133 deaths), Kaplan–Meier analysis showed improved survival for G12D (log-rank $p = 0.019$; Figure 7). Median OS was 44.8 months for G12C versus 72.4 months for G12D. After multivariable adjustment for age, sex, *STK11*, and *TP53*, the OS benefit for G12D remained statistically significant (HR = 0.63; 95% CI 0.39–0.99; $p = 0.048$; Table 4). Proportional hazards assumptions were satisfied (global $p = 0.91$). Age (HR = 1.02 per year; $p = 0.023$) and *STK11* alteration (HR = 1.48; $p = 0.042$) were additional significant predictors.

Table 4: Multivariable Cox proportional-hazards model for overall survival (OS).

Variable	HR	95% CI	z	p-value
KRAS G12D vs G12C	0.63	0.39–0.99	−1.98	0.048
Age (per year)	1.02	1.00–1.04	2.27	0.023
Sex: Male	1.01	0.70–1.46	0.05	0.960
<i>STK11</i> altered	1.48	1.01–2.16	2.03	0.042
<i>TP53</i> altered	1.41	0.99–2.01	1.91	0.056

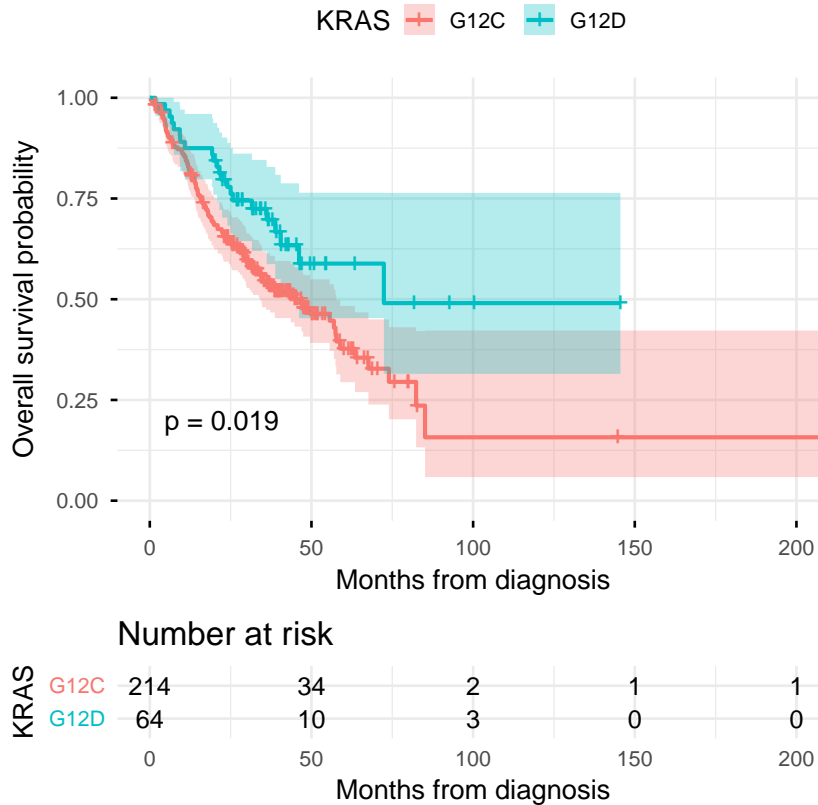


Figure 7: Kaplan–Meier overall survival curves by KRAS allele (months from diagnosis; $n = 278$; 133 deaths). Log-rank $p = 0.019$ (unadjusted). Adjusted HR for G12D = 0.63 (95% CI 0.39–0.99; $p = 0.048$; Table 4).

3.5 Sensitivity and Robustness Analyses

TMB-adjusted model. Addition of TMB (per 5 mut/Mb) as a covariate did not materially alter the allele effect: $HR_{\text{early}} = 0.39$ (95% CI 0.16–0.92); interaction HR = 3.38 (95% CI 1.21–9.44; $p = 0.020$). TMB itself was not significantly associated with TTNT in the piecewise model ($p = 0.319$).

Alternative cut-points. Piecewise models at the 25th (12.0 months), 75th (34.7 months), and 95th (65.4 months) TTNT percentiles consistently yielded early HRs below 1.0 (range:

0.19–0.83) and late HRs above 1.0 (range: 1.02–1.42), supporting directional consistency across cut-point choices, though confidence intervals widened with more extreme splits due to smaller risk sets.

Exclusion of early events (≤ 2 months). Censoring treatment changes within 2 months did not alter the primary findings: $\text{HR}_{\text{early}} = 0.41$ (95% CI 0.18–0.97); interaction $\text{HR} = 3.33$ (95% CI 1.19–9.31; $p = 0.022$).

4 Discussion

In this real-world, allele-resolved analysis of the AACR Project GENIE BPC NSCLC cohort, we found that KRAS G12C and G12D lung adenocarcinomas exhibit distinct co-mutation profiles and directionally different temporal treatment durability patterns. Although unadjusted TTNT and standard multivariable Cox models did not identify a significant overall difference between alleles, time-structured modeling revealed a statistically supported early TTNT advantage for G12D that attenuated during later follow-up. This time-varying pattern was directionally consistent across bootstrap resampling, alternative cut-points, and TMB-adjusted sensitivity analyses. Additionally, G12D was associated with significantly improved OS in a larger evaluable cohort.

4.1 Biological Context for Observed Patterns

The allele-specific molecular features observed in our cohort provide a plausible biological framework for the time-varying outcomes. G12C tumors displayed significantly higher TMB and greater enrichment of *STK11* and *KEAP1* co-mutations, findings concordant with prior translational and registry studies [Skoulidis et al., 2015, Prior et al., 2020, Zhang et al., 2022]. *STK11* and *KEAP1* alterations define immunologically cold tumor phenotypes with attenuated benefit from ICB and are associated with poorer outcomes across KRAS alleles [Skoulidis et al., 2015, Bazhenova, 2023]. The relative paucity of these co-mutations in G12D tumors may contribute to more durable early treatment responses, including to ICB-containing regimens commonly used in first-line NSCLC.

The G12D OS advantage (adjusted $\text{HR} = 0.63$; $p = 0.048$) persisted despite G12D’s lower median TMB and late-period TTNT convergence. This is noteworthy because lower TMB is generally associated with reduced immunotherapy benefit, suggesting that the co-mutation landscape — particularly the relative absence of *STK11/KEAP1* alterations — may preserve treatment responsiveness across sequential lines in G12D tumors more than TMB alone would

predict. These observations are concordant with published evidence that co-mutation context, rather than TMB in isolation, is a more reliable predictor of KRAS allele-specific ICB outcomes [Zhao et al., 2024, Cantor et al., 2025].

The late-period attenuation of G12D’s early TTNT advantage may reflect several non-mutually exclusive mechanisms: emergence of resistant subclones, clonal evolution under therapeutic pressure, exhaustion of immune-mediated tumor control, or differential downstream KRAS signaling over time. These dynamic changes would not be detectable using conventional proportional-hazards models [Désage et al., 2022, Chao and Di, 2025], underscoring the value of time-adaptive analytical frameworks for molecular subgroup analyses.

4.2 Therapeutic Context

An important consideration is that G12C-targeted inhibitors (sotorasib, adagrasib) became clinically available during the study period covered by the GENIE BPC dataset. Our analysis could not separately identify patients who received these agents. If G12C patients disproportionately accessed targeted therapies in later lines, this could contribute to the attenuation of G12D’s early durability advantage independent of biological mechanisms. Future analyses with explicit capture of allele-targeted therapy exposure will be necessary to separate treatment-era effects from underlying allele biology.

For G12D specifically, early-phase inhibitors including zoldonrasib represent the first targeted options for this subgroup [Hippensteele]. Our real-world TTNT and OS data provide pre-targeted-era benchmarks that may contextualize future comparative effectiveness analyses as G12D-directed therapies mature.

4.3 Limitations

This study has several important limitations that require careful consideration.

First and most critically, the G12D cohort in the TTNT analyses was small ($n = 32$), which substantially constrained statistical power, particularly for late-period inferences. Post-hoc power analysis using the Schoenfeld formula indicated that detecting the observed late-period HR of 1.38 with 80% power at $\alpha = 0.05$ would require approximately 489 events among patients surviving beyond 23 months, corresponding to roughly 193 G12D and 785 G12C patients. With approximately 40 late-period events observed, the achieved power for the late-period comparison was only 12.3%. Consequently, the non-significant late-period HR ($p = 0.285$) most plausibly reflects inadequate power rather than absence of a true effect, and late-period estimates should be treated as exploratory and hypothesis-generating. Confirmation of the late-period pattern

requires prospective validation in larger, allele-resolved cohorts or pooled multi-institutional analyses.

Second, TTNT is an imperfect surrogate for radiographic progression: clinician decisions to change therapy may be influenced by tolerability, patient preference, or administrative factors independent of disease progression. Nonetheless, TTNT is a widely used and pragmatically validated real-world endpoint in observational oncology research [Khozin et al., 2019, Campbell et al., 2020]. Third, incomplete or variable reporting of genomic data (CNAs, SVs, TMB, PD-L1) across institutions may introduce differential misclassification of co-mutation and biomarker variables. Fourth, unmeasured confounding by treatment selection, center-specific practice patterns, or performance status not captured in the BPC public release cannot be fully excluded despite multivariable adjustment. Fifth, OS follow-up in the BPC v2.0 public release may be incomplete or variably mature across centers, and the OS findings, while statistically significant, should be interpreted in that context.

4.4 Strengths

Strengths include the use of deeply curated, harmonized treatment timelines from GENIE BPC enabling high-resolution TTNT measurement; comprehensive co-mutation harmonization across three genomic data types; application of multiple complementary survival modeling frameworks that explicitly evaluated proportional hazards assumptions; and rigorous bootstrap internal validation demonstrating directional stability of time-varying estimates. Pre-specifying the median cut-point prior to analysis avoids data-driven selection bias that commonly inflates type-I error in piecewise modeling.

4.5 Implications and Future Directions

These findings support several practical implications. First, KRAS-mutant NSCLC should not be treated as a uniform molecular entity in clinical or research settings; allele-specific and temporally stratified outcome reporting is warranted. Second, prospective studies and registries should prespecify time-varying survival analyses and ensure sufficient allele-level sample sizes to detect dynamic effects with adequate power. Third, integrative multi-omic approaches—including immune profiling, longitudinal circulating tumor DNA sampling, and post-progression genomic characterization, are needed to mechanistically dissect the early-to-late transition in allele-specific hazards. Finally, patients with KRAS G12D should be considered high-priority candidates for G12D-directed clinical trials as targeted agents advance through development.

4.6 Conclusions

In this multi-institutional real-world analysis, KRAS G12D lung adenocarcinomas demonstrated an early TTNT durability advantage and significantly improved OS compared with G12C, despite similar overall TTNT. Time-structured survival modeling identified allele-specific hazard dynamics that conventional proportional-hazards analyses did not reveal. The early-period KRAS effect was statistically significant and bootstrap-confirmed; the late-period pattern was directionally consistent but did not reach significance, reflecting limited power from the small G12D cohort rather than evidence against the effect. These exploratory findings challenge the treatment of KRAS-mutant NSCLC as a homogeneous entity and support prospective investigation of allele-specific treatment trajectories, particularly as G12D-targeted therapeutics enter clinical practice.

Acknowledgements

We thank the AACR Project GENIE Consortium and all contributing institutions for public access to de-identified data.

Data Availability

Data are publicly available from the AACR Project GENIE BPC NSCLC v2.0-public release via cBioPortal.

Conflicts of Interest

The authors declare no conflicts of interest.

Funding

No specific funding was received for this work.

References

A Frisch, E Martin, S Y Kim, J W Riess, T Sen, and N Karim. Kras mutated nscl: Past, present, and future directions in a rapidly evolving landscape. *The Oncologist*, 30(6):oyaf153, 2025. doi:10.1093/oncolo/oyaf153.

- T K H Lim, F Skoulidis, K M Kerr, M J Ahn, J R Kapp, F A Soares, and Y Yatabe. Kras g12c in advanced nscl: Prevalence, co-mutations, and testing. *Lung Cancer*, 184:107293, 2023. doi:10.1016/j.lungcan.2023.107293. Epub 2023 Jul 13.
- A Shahnam, A Davis, L J Brown, I Sullivan, K Lin, C Ng, N Yeo, B Y Kong, T Khoo, L Warburton, I P Da Silva, W Mullally, W Xu, K O'Byrne, V Bray, A Pal, A Mersaides, M Itchins, S Arulananda, A Nagrial, S Kao, M Alexander, C K Lee, B Solomon, and T John. Real-world outcomes of non-small cell lung cancer patients harbouring kras g12c and kras g12d mutations. *Lung Cancer*, 201:108421, 2025. doi:10.1016/j.lungcan.2025.108421. Epub 2025 Feb 12.
- Bo Zhang, Jingtong Zeng, Hao Zhang, Shuai Zhu, Hanqing Wang, Jinling He, Lingqi Yang, Ning Zhou, Lingling Zu, Xiaohong Xu, Zuoqing Song, and Song Xu. Characteristics of the immune microenvironment and their clinical significance in non-small cell lung cancer patients with ALK-rearranged mutation. *Frontiers in Immunology*, 13:974581, 2022. doi:10.3389/fimmu.2022.974581. Published 2022 Sep 07.
- L Bazhenova. Exploring the role of accessory biomarkers tmb, stk11, keap1, and kras in non-small-cell lung cancer: confused, but on a much higher level. *Annals of Oncology*, 34(4):327–332, 2023. doi:10.1016/j.annonc.2023.02.013. Erratum in: *Ann Oncol*. 2023 Aug;34(8):725–726. doi:10.1016/j.annonc.2023.05.007.
- F Skoulidis, B T Li, G K Dy, T J Price, G S Falchook, J Wolf, A Italiano, M Schuler, H Borghaei, F Barlesi, T Kato, A Curioni-Fontecedro, A Sacher, A Spira, S S Ramalingam, T Takahashi, B Besse, A Anderson, A Ang, Q Tran, O Mather, H Henary, G Ngarmchamnanrith, G Friberg, V Velcheti, and R Govindan. Sotorasib for lung cancers with kras p.g12c mutation. *The New England Journal of Medicine*, 384(25):2371–2381, 2021. doi:10.1056/NEJMoa2103695. Epub 2021 Jun 4.
- P A Jänne, G J Riely, S M Gadgeel, R S Heist, S I Ou, J M Pacheco, M L Johnson, J K Sabari, K Leventakos, E Yau, L Bazhenova, M V Negrao, N A Pennell, J Zhang, K Anderes, H Der-Torossian, T Kheoh, K Velastegui, X Yan, J G Christensen, R C Chao, and A I Spira. Adagrasib in non-small-cell lung cancer harboring a kras g12c mutation. *The New England Journal of Medicine*, 387(2):120–131, 2022. doi:10.1056/NEJMoa2204619. Epub 2022 Jun 3.
- D Brazel and M Nagasaka. Divarasil in the evolving landscape of kras g12c inhibitors for nscl. *Targeted Oncology*, 19(3):297–301, 2024. doi:10.1007/s11523-024-01055-y. Epub 2024 May 13.

Alana Hippensteele. AACR 2025: Oral investigational agent Zoldonrasib elicits objective responses in patients with KRAS G12D-mutated NSCLC. URL <https://www.pharmacytimes.com/view/oral-investigational-agent-zoldonrasib-elicits-objective-responses-in-patients-with-kras->

Rui Zhao, Yang Shu, Wei Xu, Fengxian Jiang, Pancen Ran, Liying Pan, Jingliang Wang, Weihao Wang, Jing Zhao, Yahui Wang, and Guobin Fu. The efficacy of immunotherapy in non-small cell lung cancer with KRAS mutation: a systematic review and meta-analysis. *Cancer Cell International*, 24:361, 2024. doi:10.1186/s12935-024-03761-w. Published 2024 Nov 1.

A Geçgel, B Şahin Çelik, P Peker, Z S Gökdere, D Koca, B Karaca, D Nart, and E Göker. Kras g12c mutation predicts improved survival in nsccl patients receiving immunotherapy: insights from a real-world cohort. *Journal of Clinical Medicine*, 14(19):6826, 2025. doi:10.3390/jcm14196826. Published 2025 Sep 26.

A Galan-Cobo, N I Vokes, Y Qian, D Molkenline, K Ramkumar, A G Paula, M Pisegna, D J McGrail, A Poteete, S Cho, M T Do, A Karimi, Y Kong, A Solanki, A Karmokar, N Floc'h, A Hughes, R Sargeant, L Young, L Shen, G Kar, C Keshvani, C Archedera, S Hernandez, K Schlacher, J Wang, S Iyer, J Conway, M R Keddar, M Milo, I de Toma, S E Critchlow, J C Barrett, J Cosaert, A Lau, V Valge-Archer, L A Byers, S T Barry, and J V Heymach. Keap1 and stk11/lkb1 alterations enhance vulnerability to atr inhibition in kras mutant non-small cell lung cancer. *Cancer Cell*, 43(8):1530–1548.e9, 2025. doi:10.1016/j.ccell.2025.06.011. Epub 2025 Jul 10.

I de Bruijn, R Kundra, B Mastrogiacomo, T N Tran, L Sikina, T Mazor, X Li, A Ochoa, G Zhao, B Lai, A Abeshouse, D Baiceanu, E Ciftci, U Dogrusoz, A Dufilie, Z Erkoc, E Garcia Lara, Z Fu, B Gross, C Haynes, A Heath, D Higgins, P Jagannathan, K Kalletla, P Kumari, J Lindsay, A Lisman, B Leenknecht, P Lukasse, D Madela, R Madupuri, P van Nierop, O Plantalech, J Quach, A C Resnick, S Y A Rodenburg, B A Satravada, F Schaeffer, R Sheridan, J Singh, R Sirohi, S O Sumer, S van Hagen, A Wang, M Wilson, H Zhang, K Zhu, N Rusk, S Brown, J A Lavery, K S Panageas, J E Rudolph, M L LeNoue-Newton, J L Warner, X Guo, H Hunter-Zinck, T V Yu, S Pilai, C Nichols, S M Gardos, J Philip, AACR Project GENIE BPC Core Team, AACR Project GENIE Consortium, K L Kehl, G J Riely, D Schrag, J Lee, M V Fiandalo, S M Sweeney, T J Pugh, C Sander, E Cerami, J Gao, and N Schultz. Analysis and visualization of longitudinal genomic and clinical data from the aacr project genie biopharma collaborative in cbiportal. *Cancer Research*, 83(23):3861–3867, 2023. doi:10.1158/0008-5472.CAN-23-0816. Epub 2023 Jul 31.

- S. Khozin, G. M. Blumenthal, and R. Pazdur. Real-world data for clinical evidence generation in oncology. *Nature Reviews Clinical Oncology*, 16:73–74, 2019. doi:10.1038/s41571-018-0117-4.
- Brian A. Campbell, Jeremy J. Scarisbrick, Youn H. Kim, Ryan A. Wilcox, Christopher McCormack, and H. Miles Prince. Time to next treatment as a meaningful endpoint for trials of primary cutaneous lymphoma. *Cancers*, 12(8):2311, 2020. doi:10.3390/cancers12082311. Published 2020 Aug 17.
- Aacr project genie: 10-year cohort summary. AACR White Paper, 2023. URL <https://www.aacr.org/professionals/research/aacr-project-genie/>.
- AACR Project GENIE Consortium. Aacr project genie: Powering precision medicine through an international consortium. *Cancer Discovery*, 7(8):818–831, 2017. doi:10.1158/2159-8290.CD-17-0151. Epub 2017 Jun 1.
- Terry Therneau. *A Package for Survival Analysis in R*, 2023. URL <https://CRAN.R-project.org/package=survival>.
- Alboukadel Kassambara, Marcin Kosinski, and Przemyslaw Biecek. *survminer: Drawing Survival Curves using ggplot2*, 2019. URL <https://CRAN.R-project.org/package=survminer>.
- Hadley Wickham, Romain François, Lionel Henry, and Kirill Müller. *dplyr: A Grammar of Data Manipulation*, 2023. URL <https://CRAN.R-project.org/package=dplyr>.
- F Skoulidis, L A Byers, L Diao, V A Papadimitrakopoulou, P Tong, J Izzo, C Behrens, H Kadara, E R Parra, J R Canales, J Zhang, U Giri, J Gudikote, M A Cortez, C Yang, Y Fan, M Peyton, L Girard, K R Coombes, C Toniatti, T P Heffernan, M Choi, G M Framp-ton, V Miller, J N Weinstein, R S Herbst, K K Wong, J Zhang, P Sharma, G B Mills, W K Hong, J D Minna, J P Allison, A Futreal, J Wang, I I Wistuba, and J V Heymach. Co-occurring genomic alterations define major subsets of KRAS-mutant lung adenocarcinoma with distinct biology, immune profiles, and therapeutic vulnerabilities. *Cancer Discovery*, 5(8):860–877, 2015. doi:10.1158/2159-8290.CD-14-1236. Epub 2015 Jun 11.
- I A Prior, F E Hood, and J L Hartley. The frequency of Ras mutations in cancer. *Cancer Research*, 80(14):2969–2974, 2020. doi:10.1158/0008-5472.CAN-19-3682. Epub 2020 Mar 24.
- D J Cantor, H Nimeiri, L Horn, M West, R Ben-Shachar, I Huerga, J D Patel, and C Aggarwal. Outcomes following first-line immune checkpoint inhibitors with or without chemotherapy stratified by KRAS mutational status: a real-world analysis in patients with advanced

NSCLC. *Clinical Lung Cancer*, 26(6):503–510.e4, 2025. doi:10.1016/j.clc.2025.05.007. Epub 2025 May 28.

Anne-Laure Désage, Camille Léonce, Aurélie Swalduz, and Sandra Ortiz-Cuaran. Targeting KRAS mutant in non-small cell lung cancer: novel insights into therapeutic strategies. *Frontiers in Oncology*, 12:796832, 2022. doi:10.3389/fonc.2022.796832.

C H Chao and Y P Di. Mechanisms and current advances in treating KRAS-mutated lung cancer. *Chinese Medical Journal Pulmonary & Critical Care Medicine*, 3(3):149–163, 2025. doi:10.1016/j.pccm.2025.08.001. Published 2025 Sep 16.